Difference between Non-Newtonian Carreau and Casson Blood Viscosity Models to Predict Hemodynamics in Idealized Eccentric Arterial Stenosis: Large Eddy Simulation Modeling

Shamudra Dey
Department of Mechanical Engineering, Shahjalal University of Science and Technology

Tahsin Ibtida
Department of Mechanical Engineering, Shahjalal University of Science and Technology

Chandan Kumar Roy
Department of Mechanical Engineering, Shahjalal University of Science and Technology

Nuruzzaman Sakib
Department of Mechanical Engineering, Shahjalal University of Science and Technology

https://doi.org/10.5109/4102499

出版情報：Proceedings of International Exchange and Innovation Conference on Engineering & Sciences (IEICES). 6, pp.249-257, 2020-10-22. Interdisciplinary Graduate School of Engineering Sciences, Kyushu University
バージョン：
権利関係：

Difference between Non-Newtonian Carreau and Casson Blood Viscosity Models to Predict Hemodynamics in Idealized Eccentric Arterial Stenosis: Large Eddy Simulation Modeling

Shamudra Dey, Tahsin Ibtida, Chandan Kumar Roy, Nuruzzaman Sakib
Department of Mechanical Engineering, Shahjalal University of Science and Technology, Sylhet-3114, Bangladesh.
Corresponding author email: shamudra-mee@student.sust.edu

ABSTRACT: *Atherosclerosis is the principal cause of heart diseases and hemodynamics is a vital aspect. For current work, Large Eddy Simulation (LES) technique is chosen to visualize the variation between non-Newtonian Carreau and Casson viscosity models to simulate hemodynamics in idealized version of 75% eccentrically occluded artery. In the LES methodology, although the unsolved movements are rendered using the Smagorinsky-Lily model, the full resolution of large-size movements is achieved. Considering the swirl component of blood, a unique parabolic and pulsatile inlet velocity boundary condition is created to represent a realistic blood flow. By using proposed framework, the precise blood flow configuration and turbulent characteristics of the circulatory system are represented in a specific design. It was observed that the Casson model projected greater blood flow instability than the Carreau model, whereas the Carreau model predicted higher fluctuations in speed, pressure, and wall shear stress. High speed, pressure and WSS variations are responsible for a psychological problem termed arterial murmur.*

Keywords: Atherosclerosis; Hemodynamics, Stenosis; Large Eddy Simulation; Wall shear stress

1. INTRODUCTION

Heart is the most essential organ of the human body to transport blood in the active vascular system [1]. Atherosclerosis or arterial stenosis is a particular form of heart disease which is predominantly induced by accumulation of LDL-cholesterol, vascular endothelial cells, macrophages as well as calcium in the inner layer of plaque-forming vessels and alters the flow of blood from laminar to turbulent. While data suggests that nearly 80% of the stenosis are eccentric, the designs used in the studies mainly indicate that the artery is symmetrically affected by stenosis. Comprehension of blood circulation hemodynamics is of particular significance in the estimation of the heart disease development hypothesis. The probability that hemodynamic influences may be associated with production and progression of atherosclerosis has stimulated the study of arterial stenosis flow [2, 3]. In addition, a non-invasive screening tool that is widely used in clinical service to assess the magnitude of stenosis relies on the severity of local turbulent pressure variations as a possible cause of arterial murmurs [4].

In recent years, much emphasize has been given on the hemodynamics studies considering blood as Newtonian and homogenous fluid. From several research, it is evident that, blood is indeed a non-Newtonian visco-elastic fluid which is incompressible [5-7]. Johnston et al. [8, 9] made a study of five different non-Newtonian blood viscosity models, (i) Casson model (ii) Power-law (iii) Carreau model (iv) Walburn-Schneck and (v) Generalized power-law model, and the results indicate that the effects on shear stress were substantial for the adaptation of various models. Neofytou et al. [10-12] explored with three separate models, namely (i) Casson Model (ii) Power-law Model and (iii) Quemada Model, for blood flow study in sudden extension, arterial stenosis and aneurysm. There was a correlation in behavior between the Quemada and Casson models, although the Power-law did not indicate comparable behavioral patterns. Molla & Paul [13] researched with LES model of intermittent pulsatile blood circulation using various forms of non-Newtonian blood flow viscosity models, namely, (i) Power-law, (ii) Carreu, (iii) Quemada, (iv) Cross and (v) Modified Casson, and explored the transitional flow in the event of arterial stenosis.

Large Eddy Simulation is being used as a methodology for this computational fluid dynamics (CFD) analysis, which is a numerical method used to depict turbulence in CFD. The technique resolves the Navier-Stokes equation numerically employing low-pass filtration, space filtration, and really quite efficient laminar to transition identification, making it a perfect for this objective. As few studies are related to the prediction of hemodynamics incorporating large eddy simulation, the primary objective of this research work is to visualize the variation between non-Newtonian Carreau and Casson viscosity models to simulate hemodynamics in idealized version of 75% eccentrically occluded artery. The research is intended to better characterize non-axisymmetric arterial stenosis for non-Newtonian blood viscosity model.

2. METHODOLOGY

2.1 Model Construction

In this particular work, an idealized artery having 75% occlusion has been considered. The total span of the idealized vessel is 27D or 540 mm, where diameter D=20mm. In this particular model, upstream region is 4D, stenosis region is 2D and the downstream region is 21D. The stenosis is created using a specific cosine formula, where, δ_c=0.25, ensuring a 75% stenosis generation in the idealized artery model. The consistent removal of the cross-sectional region induced by the relation inside the vessel gives a precise description of the physiological type of arterial stenosis. Similar idealized artery models have been utilized in previous studies [14, 15].

$$\frac{r(Z)}{R} = 1 - \delta_C[1 + \cos\left(\frac{Z\pi}{D}\right)], \text{-D} \leq Z \leq D \quad (1)$$

A figure (Fig. 1) has been provided to describe the idealized artery model having 75% eccentric stenosis.

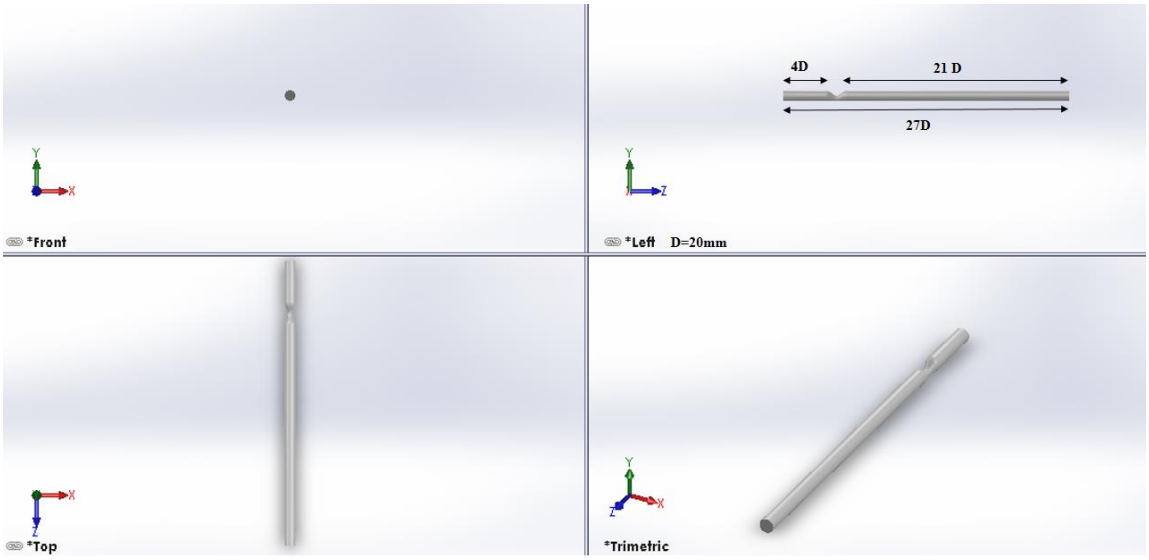

Fig. 1. Solid geometry model of idealized artery having 75% eccentric arterial stenosis

2.2 Computational Domain Discretization

ANSYS ICEM CFD grid generation tool is utilized to discretize computational domain of the current research. Triangular grid has been developed with a fairly low skewness and a relatively high orthogonal quality. Three levels of inflation were applied to the surface of the artery. As a consequence, the mesh is condensed in the stenosis area, after which the flow separation tends to occur.

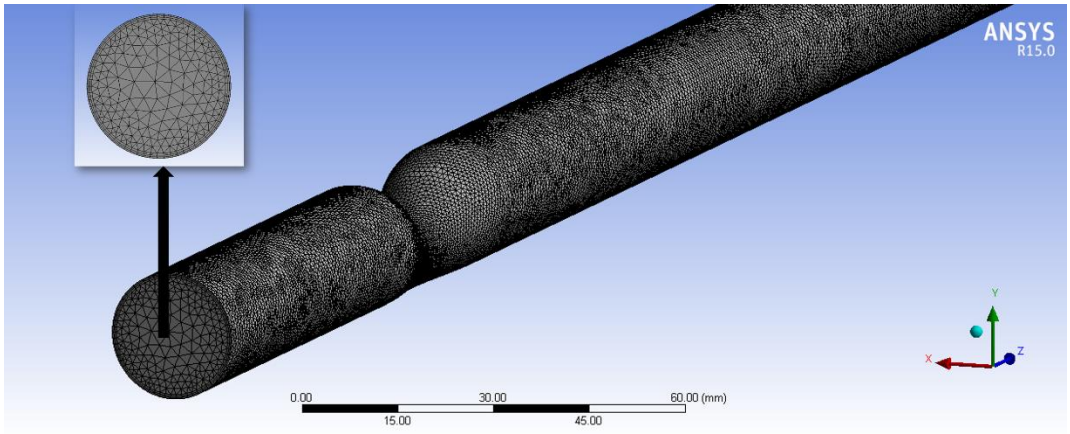

Fig. 2. Illustration of generation of grid utilizing ANSYS ICEM CFD Meshing tool

2.3 Governing Equations

The main comprehensive framework for fluid dynamics is the Navier Stokes (NS) formulas. These are the conservation rules for the 3D flow:

Continuity equation: $\nabla.\bar{U} = 0;\ \bar{U} = \frac{\partial u}{\partial x} + \frac{\partial v}{\partial y} + \frac{\partial w}{\partial z}$ (2)

N-S equation: $\frac{\partial \bar{U}}{\partial t} + \bar{U}.\nabla\bar{U} = -\frac{\Delta P}{\rho} + \mu\nabla^2\bar{U}$ (3)

Navier-Stokes filtered movement formulae for non-Newtonian fluid flow can be presented as [16]:

$$\frac{\partial \bar{u}_j}{\partial x_j} = 0 \quad (4)$$

$$\frac{\partial \rho\bar{u}_i}{\partial t} + \frac{\partial \rho\bar{u}_i\bar{u}_j}{\partial x_j} = -\frac{\partial \bar{p}}{\partial x_i} + \frac{\partial}{\partial x_j}\left[\mu(|\dot{\gamma}|)\left(\frac{\partial \bar{u}_i}{\partial x_j} + \frac{\partial \bar{u}_j}{\partial x_i}\right)\right] - \frac{\partial \tau_{ij}}{\partial x_j} \quad (5)$$

Here, $\mu(|\dot{\gamma}|)$ is the blood viscosity, that depends on the shear rate.

In the present Large Eddy Simulation study, The Smagorinsky-Lily model [17] is the most popular and still widely used model for subgrid-scale stresses, based on the assumption of eddy viscosity as:

$$\tau_{ij} - \frac{1}{3}\delta_{ij}\tau_{kk} = -2v_{sgs}\bar{S}_{ij} \quad (6)$$

As a whole, the Smagorinsky-Lily model emerges as:

$$\tau_{ij} - \frac{1}{3}\delta_{ij}\tau_{kk} = -2(C_s\Delta)^2|\bar{S}|\bar{S}_{ij} = -2(C_s)^2\beta_{ij} \quad (7)$$

Here, $\beta_{ij} = \Delta^2|\bar{S}|\bar{S}_{ij}$. The C_s value is 0.12 for both non-Newtonian Carreau and Casson blood viscosity model according to the findings of Mollah [16].
Two non-Newtonian blood viscosity model Carreau and Casson have been compared in the present study. The carreau model is given by:

$$\mu(|\dot{\gamma}|) = \mu_\infty + (\mu_0 - \mu_\infty)[1 + (\lambda\dot{\gamma})^2]^{(n-1)/2} \quad (8)$$

Here, $\mu_0 = 0.056\ Pa.s$, which is viscosity of blood at shear rate of zero, Time constant $\lambda = 3.313$, γ is the instantaneous rate of shear and n = 0.3568.
On the other hand, the Casson blood viscosity model is given by:

$$\mu = \frac{\mu_\infty^2}{\dot{\gamma}} + \frac{2\mu_\infty N_\infty}{\sqrt{\dot{\gamma}}} + N_\infty^2 \quad (9)$$

$$N_\infty = \sqrt{\mu_p(1 - Hct)^{-0.25}} \quad (10)$$

$$\mu_\infty = \sqrt{(0.625Hct)} \quad (11)$$

In case of blood, μ_p=*0.00145 Pa.s* and Hct =*0.4*. It is to be mentioned that, $\tau_y = \mu_\infty^2$, called as yield stress. $K_c = N_\infty$ is also defined as consistency index.

2.4 Boundary Conditions

Blood flow in human circulatory system is pulsatile and parabolic in nature. Also, as the heart is bent on its own axis, the arterial blood flow is spiral in characteristics [18, 19]. The velocity at inlet is a time varying periodic profile with consideration of swirl part in flow of blood (Fig. 3). At the time of systole, the sinusoidal wave has the highest speed of 0.5 m/s, and at the time of diastole, the lowest speed is 0.1 m/s. The time span of each period is 0.5s. The peak systole is at t_1=0.11 s. and mean diastole is at t_2=0.36 s.

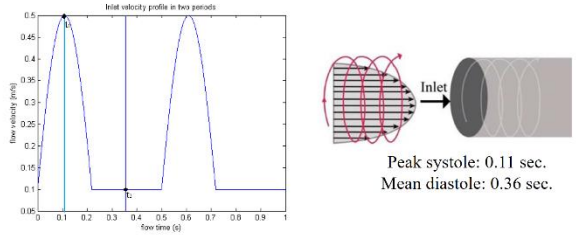

Fig. 3. Time dependent inflow boundary condition

A no-slip boundary condition has been employed on the artery wall as the elastic property of artery is negligible. On the other hand, 100 mm Hg (13332 Pa.) has been considered as static gage pressure at the outlet considering the average of highest pressure of 120 mm Hg and lowest pressure of 80 mm Hg in stable condition.

2.5 Numerical Simulation Procedure

ANSYS Fluent 15.0 utilizes Finite Volume Method to resolve fundamental equations computationally by converting them into the system of algebraic equations and it is an iterative process. Velocity is paired with pressure by using SIMPLE method. The inlet velocity boundary condition, written in C-language later interpreted as the User Defined Function in Fluent software. For the finer time step size of 0.005s, 100 time steps have been considered with 100 iterations each time step. For every time step, the residual downs gradually and the convergence criteria was set to 1e-03 for continuity and 1e-04 for x, y, z velocity.

2.6. Validation and Verification

As a new inlet velocity boundary profile has been developed, it is essential to analyze its performance with a well-established experimental study. In the current work, the study is compared with the LDA (Laser Doppler Anemometer) based research of Ahmed et al, who experimented dye-flow field in an axisymmetrically constricted tube for Re=600 [14]. Also, the study has been contrasted with the findings Direct Numerical Simulation study of Varghese [20]. As expected, few differences were observed due to the difference in between different mathematical models and experimental setup.

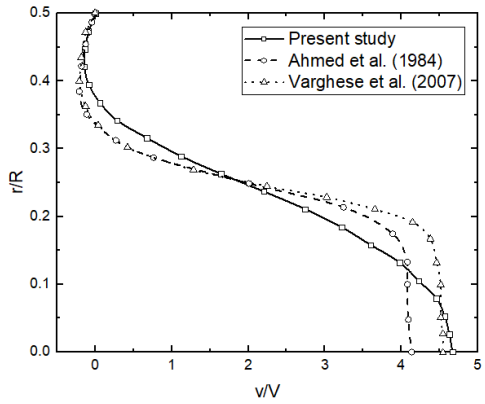

(i) Z=1D

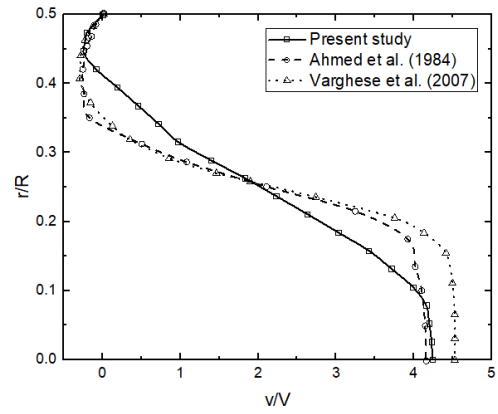

(ii) Z=1.5D

Fig. 4. Comparison of axial velocity profile at (i) Z=1D and (ii) Z=1.5D for peak flow (Re=600)

The verification of a computational study includes both grid independence test and time step independence test. Gird 1 (coarse), grid 2 (medium) and grid 3 (fine) comprises of 0.16 million, 0.45 million and 0.91 million elements respectively. Fig. 5 shows the grid independence test of current research at mean diastole and fine grid was selected for all CFD simulations to achieve reliable results.

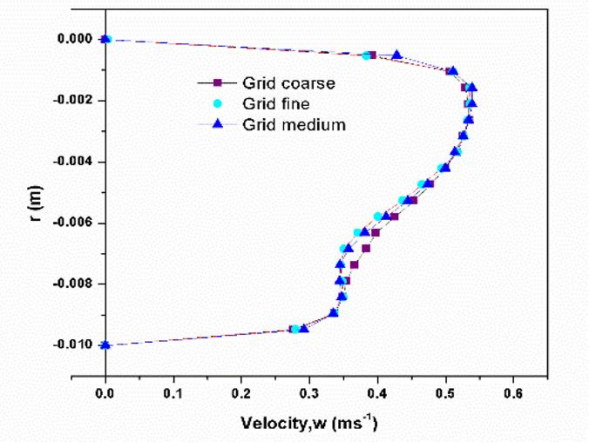

Fig. 5. Grid independence test at throat of stenosis

In case of time step independence test, two time step sizes were considered: 0.005s and 0.01s. Between them, the finer time step size of 0.005s was considered to achieve accurate result in the numerical study. Fig. 6 depicts the time step independence test at peak systole.

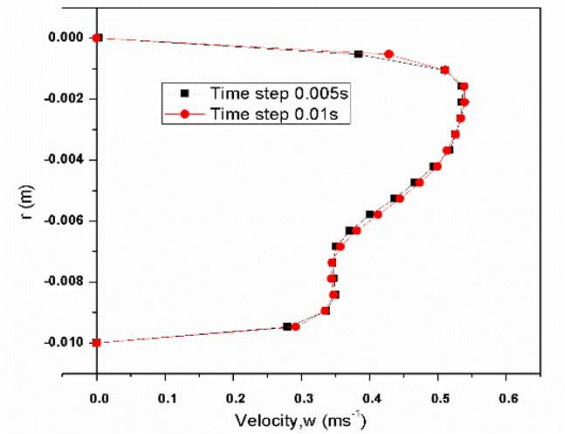

Fig. 6. Time step independence test at stenosis throat

3. RESULTS AND DISCUSSION

Numerous flow properties have been monitored in order to compare and contrast the blood circulation in eccentric stenosis in the idealized blood vessel model for the non-Newtonian Careeau and Casson models. The key purpose of this is to examine the corresponding improvements in the properties of blood flow. The results and findings have been discussed.

3.1 SGS Eddy Viscosity

In LES turbulence analysis, a sub-grid approach is used to assess the effect of unsolved tiny eddies in flow dynamics. The connection between SGS eddy viscosity and two distinct non-Newtonian blood viscosity models (Casson and Carreau) is shown in Fig. 7. SGS eddy viscosity is indeed a significant predictor of turbulence in the flow. As from figure, it is certain that the Carreau model projected higher (3.27e+003 Pa.s) SGS eddy viscosity relative to the Casson model (3.046e+003 Pa.s). The Casson model has identified certain upstream eddies that are not apparent in the case of the Carreau model.

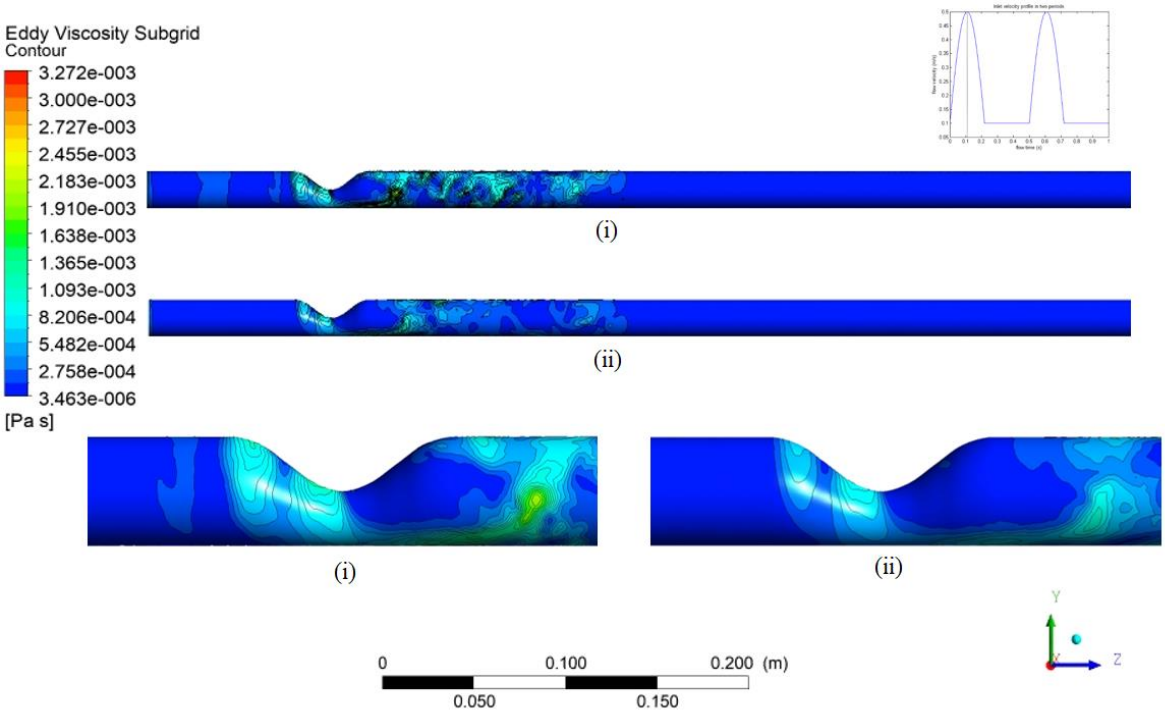

Fig. 7. Comparison of SGS eddy viscosity contour at peak systole (t_1=0.11s) for (i) Casson & (ii) Carreau model (stenosis region is zoomed)

3.2 Vorticity

Fig. 8 presents a correlation of the contour of vorticity at the highest systole for (i) Casson and (ii) Carreau model. For the Casson model, Vorticity is observed to be higher (2.414e+003 s^{-1}) than the Carreau model. Therefore, the Casson model expected greater blood flow instability

owing to eccentric thrombosis on the idealized artery. Also, vortices have been observed in the pre stenotic region in case of Casson model which is absent in the Carreau model.

3.3 Flow Visualization and Corresponding Graphs

Fig. 9 illustrates the contrasting velocity of the mean diastole of (i) the Casson model and (ii) the Carreau model. The Carreau model predicted a higher velocity (0.54 m/s) than the Casson model (0.53 m/s), but the dissipation of velocity is faster in the Carreau model. From this result, it has been shown that the span of the recirculation period is extended in the non-Newtonian Casson model; this is a disturbing pathological trend, because the blood in the recirculation region has been allowed to flow for a long period and is stagnant in that region and may induce blood clotting and maybe even thrombosis.

Fig. 10 depicts a correlation of the velocity streamline at the highest systole for the (i) Casson & (ii) Carreau model. Vortices were identified for both simulations, but the Casson model projected higher velocity in the downstream area. In the Casson model, the blood spiral part could not be recovered while in the Carreau model, the blood flow is able to recover its spiral part.

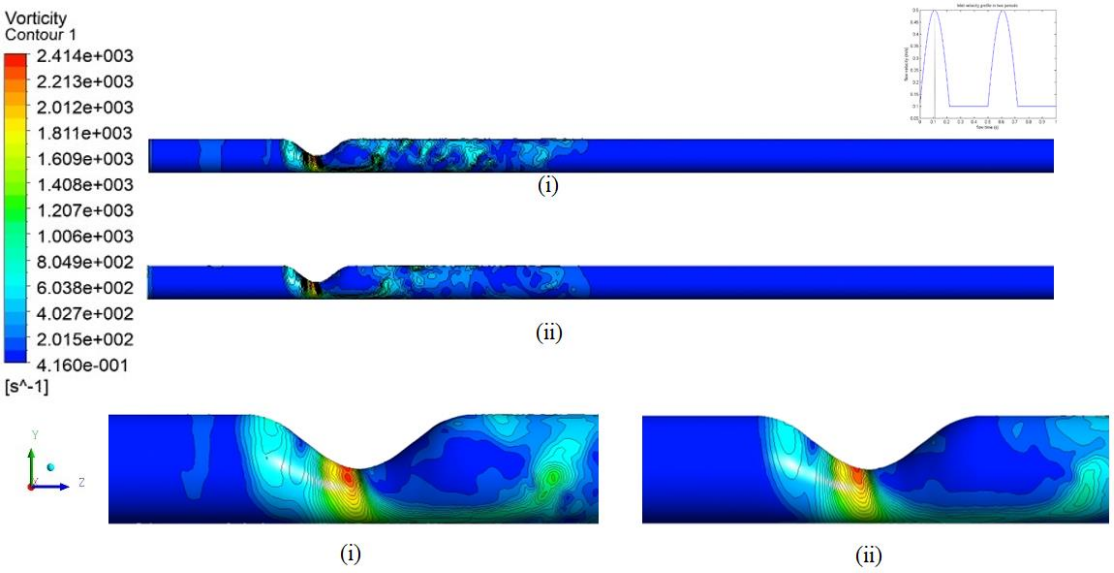

Fig. 8. Contrast of vorticity contour at peak systole for (i) Casson & (ii) Carreau model (stenosis region is zoomed)

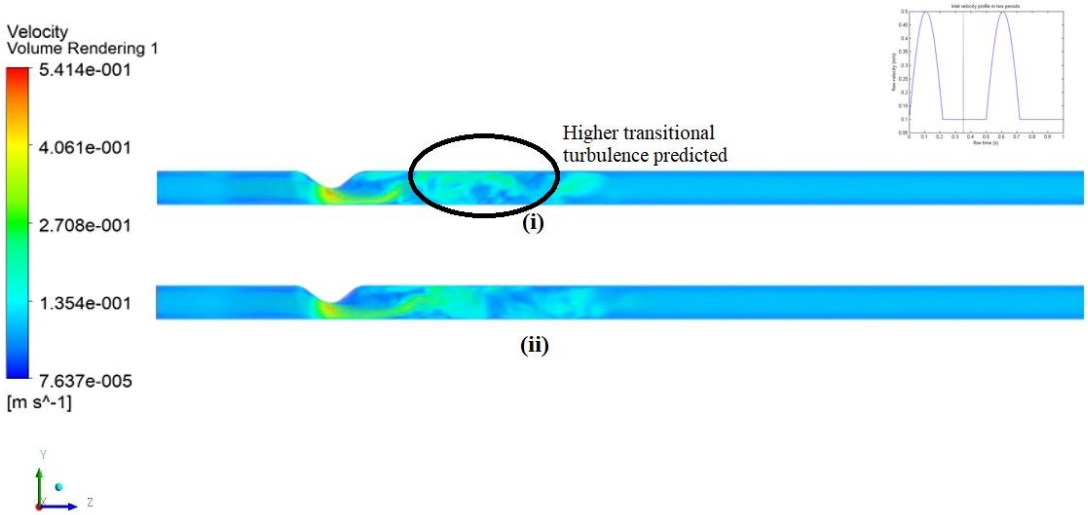

Fig. 9. Contrast of velocity rendering at mean diastole (t_2=0.36s) for (i) Casson & (ii) Carreau viscosity model

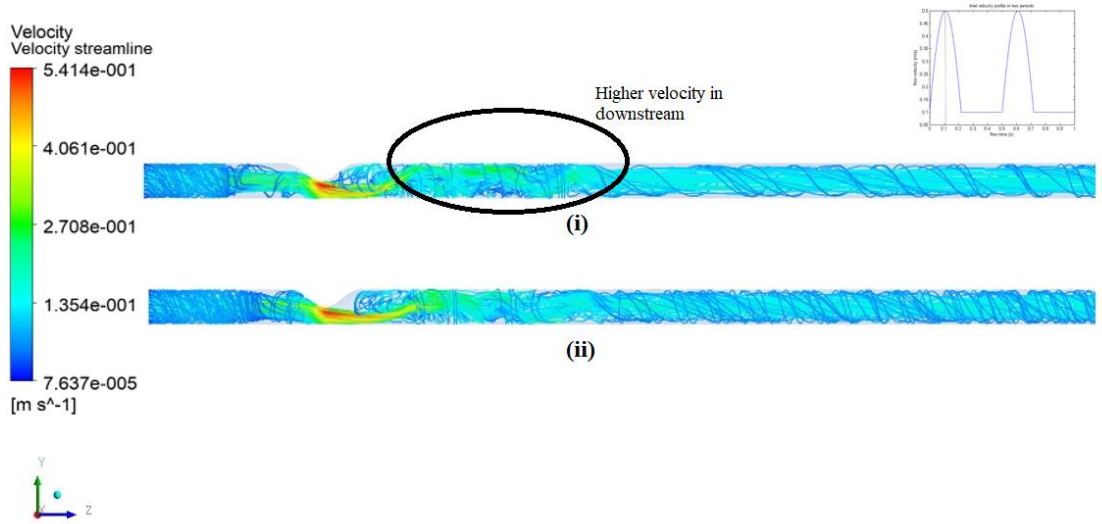

Fig. 10. Contrast of velocity streamline at peak systole (t_1=0.11s) for (i) Casson and (ii) Carreau viscosity model

3.4 Pressure

Fig. 11 illustrates a description of the pressure contour at the highest systole for both non-Newtonian blood viscosity models: the Casson & Carreau model. For the Carreau model, higher pressure (13432 Pa) is found in the pre-stenotic area than the Casson model (13420 Pa). Nonetheless, for the Casson model, high pressure contours can be visualized for some post-stenotic region, which is absent in the system of the Carreau model.

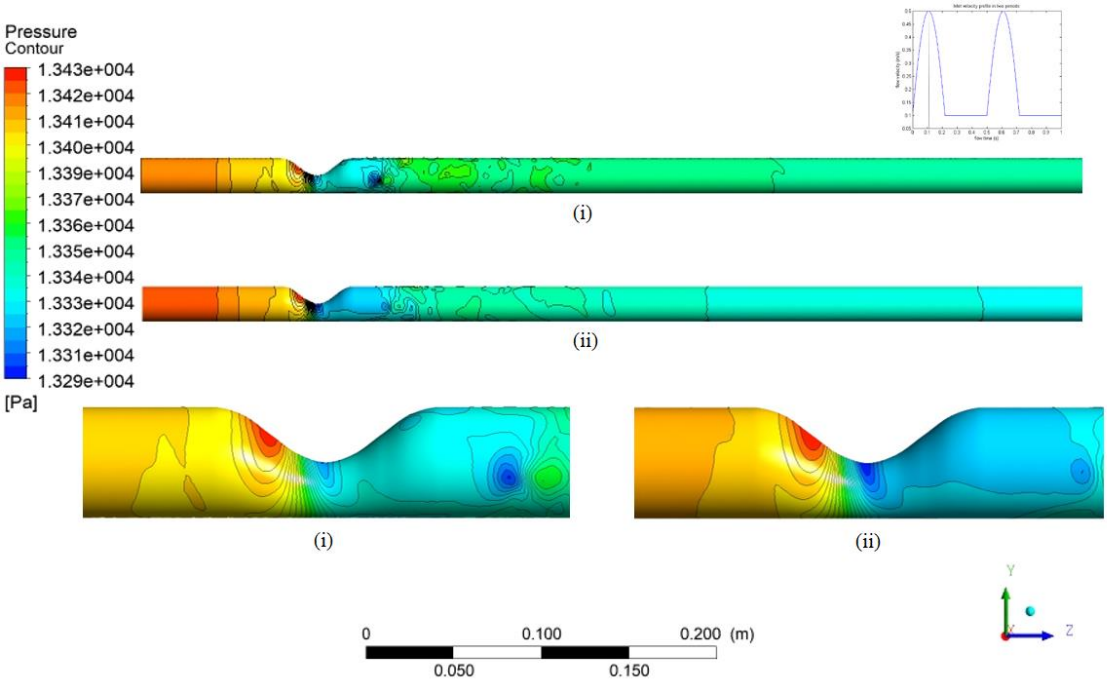

Fig. 11. Contrast of pressure contour at peak systole (t_1=0.11s.) for non-Newtonian (i) Casson and (ii) Carreau model

Fig. 12 provides a comparison of peak systolic pressure for non-Newtonian Casson and Carreau models. The disparity between these two types of non-Newtonian blood viscosity in terms of pressure vs. z is quite minimal. In both situations, the pressure decrease in the stenotic region occurred. Nonetheless, the Carreau model projected a higher pressure decrease on the centerline wall and therefore the gradient of the graph is steeper for the Carreau model. High pressure alterations are accountable for post-stenotic clotting owing to arterial disruption and are often a possible cause of medical disorder called arterial murmur.

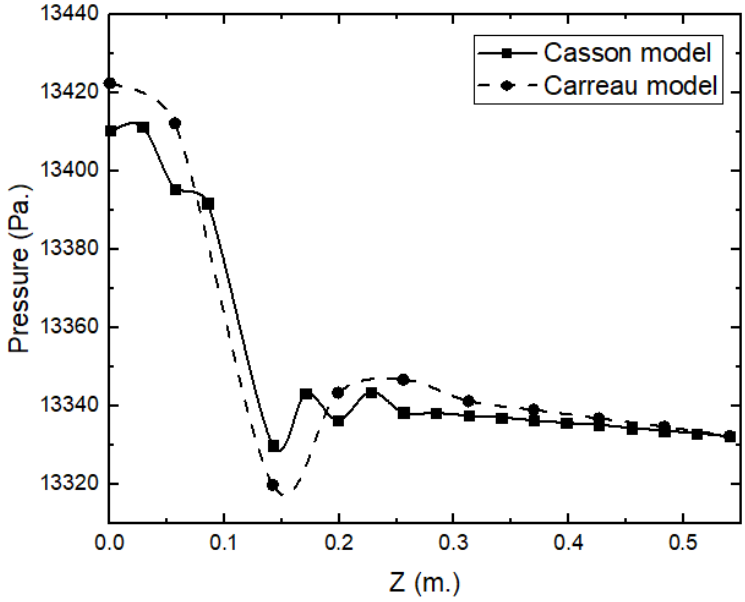

Fig. 12. Representation of pressure vs z graph at peak systole (t_1=0.11s)

3.5 Wall Shear Stress

WSS within the arteries is defined as shear stresses at the fluid layer at the inner walls of the arteries. Fig. 13 is a contrast of the wall shear stress at the highest systole for both the Casson & Carreau model. High wall shear stress (WSS) has been witnessed for the non-Newtonian Carreau model.

Fig. 14 is a contrast of the shear stress on the lower side of the wall. Wall shear stress decline occurs in the post-stenotic field, but the Carreau model's wall shear stress fall is steeper than the Casson model in all cases. The Carreau model expected higher shear stress on the lower side. The Carreau model also showed higher variations in downstream shear stress on the wall. The graphs have projected four times greater wall shear stress at the stenosis region than the stable condition.

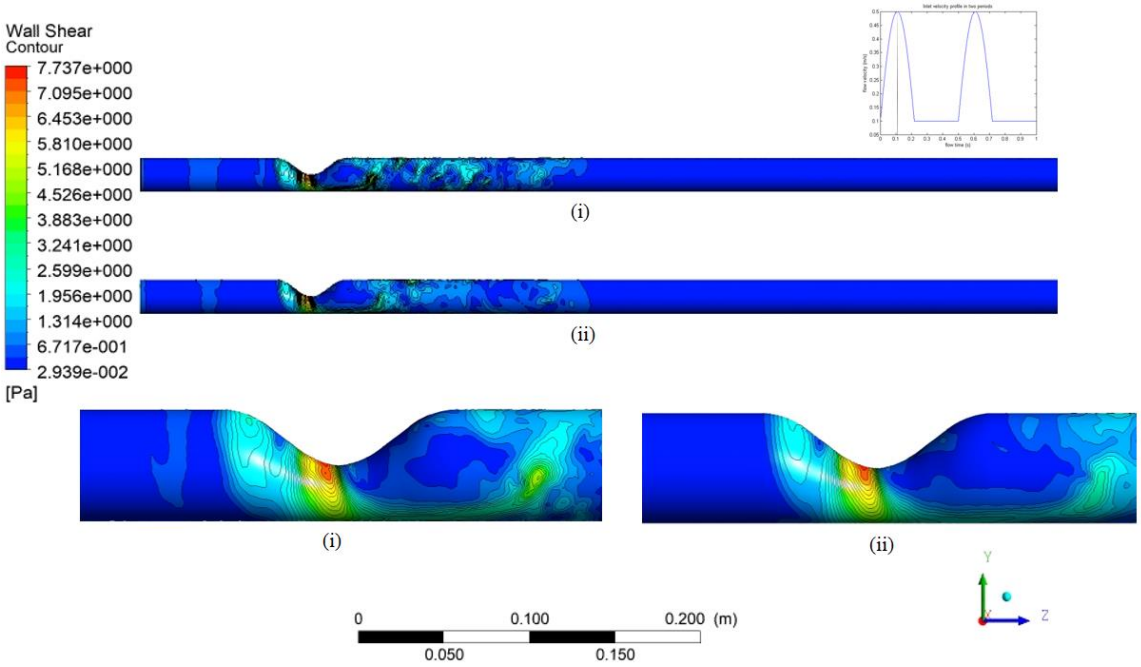

Fig. 13.Contrast of wall shear stress contour at peak systole (t_1=0.11s) for the (i)Casson & (ii) Carreau model (stenosis region is zoomed)

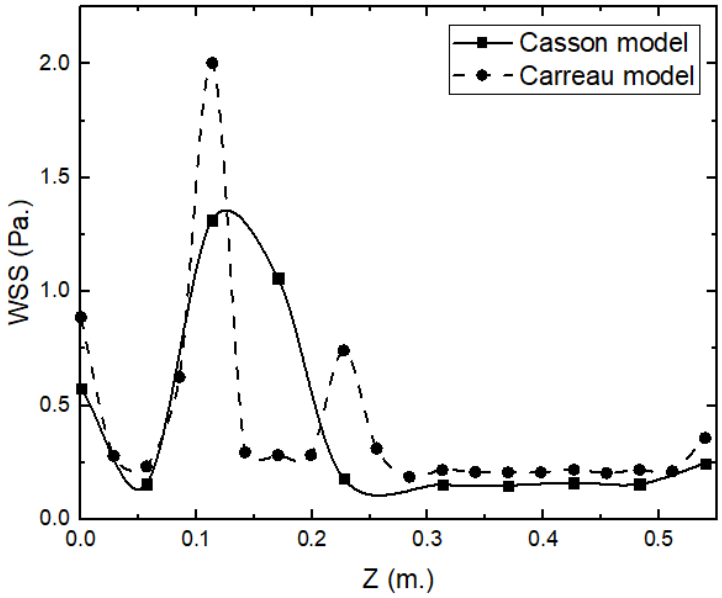

Fig. 14.Representation of WSS vs. z graph at peak systole (t_1=0.11s)

4. LIMITATIONS

While Large Eddy Simulation turbulence analysis is seen to be an efficient method for bio-fluid applications, this comprehensive analysis is restricted to a few restrictions. Firstly, the 3D geometry design of the present research is idealized. A much more accurate vessel can be modeled using patient-specific CT scan information. Further, this specific analysis did not recognize the elastic properties of the artery wall and the relationship of fluid-structure was not addressed. There are drawbacks that can be noted in the up-coming research.

5. CONCLUDING REMARKS

In this study, disparities between the non-Newtonian Casson model and the Carreau model were discussed in terms of predicting hemodynamics in idealized eccentric arterial stenosis incorporating Large Eddy Simulation turbulence modelling. The spiral component of blood circulation was considered with pulsatile and parabolic characteristics of blood flow. The Carreau model reported greater maximum SGS eddy viscosity while the vorticity of the non-Newtonian Casson model was reported to be stronger than that of the Carreau model. Nevertheless, the Carreau model expected higher velocity, pressure and wall shear stress changes than the Casson model, which is associated with a psychological disorder regarded as arterial murmur. Therefore, this study has provided a valuable and comprehensive understanding about the blood flow dynamics for two different non-Newtonian Casson and Carreau models.

6. ACKNOWLEDGEMENTS

The authors would want to mention the CFD modeling system of the ‘CAD CAM Simulation Laboratory’ of the Department of Mechanical Engineering, Shahjalal University of Science & Technology. The authors also state that they have no recognized conflicting financial interests or personal relations that may have had an effect on the research presented in this article.

7. REFERENCES

[1] S.H. Marwan, M. Todo, Biomechanical Analysis of Hypertrophic Cardiomyopathy Behavior of Human Heart using Dynamic Finite Element Method, Proceedings of International Exchange and Innovation Conference on Engineering & Sciences (IEICES) 5 (2019) 60-62.

[2] S. Ahsas, S. Tiwari, Numerical Simulation of Blood Flow through Asymmetric and Symmetric Occlusion in Carotid Artery, Proceedings of the 3rd International Conference on Fluid Flow, Heat and Mass Transfer (FFHMT), Ottowa, Canada (2016).

[3] R. Padukkage, T. Barber, Effect of Non-Axisymmetry in Arterial Stenoses, 19th Australasian Fluid Mechanics Conference, Melbourne, Australia (2014)

[4] R. S. Lees, C. F. Dewey, Phonoangiography: a new noninvasive diagnostic method for studying arterial disease, Proceedings of the National Academy of Science, 67(2) (1970) 935–942.

[5] Y. C. Fung, Biomechanics: Circulation, 2nd edition, Springer, 1997.

[6] S. A. Berger, L.-D. Jou, Flows in stenotic vessels, Annu. Rev. Fluid Mechanics 32 (2000) 347–382.

[7] C. R. Huang, W. D. Pan, H. W. Chen, A. L. Copley, Thixotropic properties of whole blood from healthy human subjects, Biorheology 24 (1987) 795–801.

[8] B. M. Johnston et al., Non-Newtonian blood flow in human right coronary arteries: steady state simulations, J. Biomechanics 37 (2004) 709–720.

[9] B. M. Johnston et al., Non-Newtonian blood flow in human right coronary arteries: transient simulations, J. Biomechanics 39 (2006) 1116–1128.

[10] P. Neofytou, S. Tsangaris, Flow effects of blood constitutive equation in 3D models of vascular anomalies, Int. J. Numer. Meth. Fluids 51 (2006) 489–510.

[11] P. Neofytou, D. Drikakis, Effects of blood models on flows through a stenosis, Int. J. Numer. Meth. Fluids 43 (2003) 597–635.

[12] P. Neofytou, D. Drikakis, Non-Newtonian flow instability in a channel with a sudden expansion,

J.Non-Newtonian Fluid Mechanics 111 (2003) 127–150.
[13] M.M. Mollah, M.C. Paul, LES of non-Newtonian physiological blood flow in a model of arterial stenosis, Medical Engineering and Physics 34 (8) (2012) 1079-1087.
[14] S. A. Ahmed, D. P. Giddens, Flow disturbances measurements through a constricted tube at moderate Reynolds number, J. Biomechanics 16 (1983) 955–963.
[15] M. D. Deshpande et al., Steady laminar flow through modelled vascular stenosis, J. Biomechanics 9 (1976) 165–174.
[16] M.M. Mollah, LES of Pulsatile Flow in the Models of Arterial Stenosis and Aneurysm, Ph.D. thesis, Department of Mechanical Engineering, University of Glasgow Glasgow, 2009.
[17] J. Smagorinsky, General circulation experiment with the primitive equations.i. the basic experiment, Monthly Weather Rev. 91 (1963) 99–164.
[18] P.A. Stonebridge, and C.M. Brophy, Spiral laminar flow in arteries, Lancet 338 (1991).
[19] P.A. Stonebridge et al, Spiral laminar flow in vivo. Clinical Science 91 (1996) 17–21.
[20] S. S. Varghese et al., Direct numerical simulation of stenotic flows. Part 2. Pulsatile flow, J. Fluid Mechanics 582 (2007) 281– 318.